

PLASMONIC-ELECTROCHEMICAL DUAL MODALITY MICROFLUIDIC SENSOR FOR CANCER BIOMARKER DETECTION

Md. Azahar Ali, Shawana Tabassum, Qiugu Wang, Yifei Wang, Ratnesh Kumar and Liang Dong
Department of Electrical and Computer Engineering, Iowa State University, Ames, Iowa, USA

ABSTRACT

A dual-modality microfluidic immunosensor is reported for the detection of cancer biomarker proteins using graphene oxide assembled periodic gold nanoposts array. The sensor uniquely provides both electrochemical and surface plasmon resonance (SPR) signatures on a single platform. Sensitivities for both electrochemical and SPR detection schemes are found to be $3.94 \mu\text{A}/\mu\text{M}/\text{cm}^2$ in a range of 1×10^{-15} M to 0.1×10^{-6} M, and $2.9 \text{ nm}/\mu\text{M}/\text{cm}^2$ in a range of 1×10^{-15} M to 1×10^{-9} M, respectively, for the detection of epidermal growth factor receptor 2 (ErbB2) breast biomarker. The present dual-modality sensor approach enables improved detection reliability and precision, and reduced false reads.

INTRODUCTION

Early diagnostics of cancer biomarker requires a sensor to provide high sensitivity, specificity and reproducibility, as well as easy operation with minute sample consumptions [1]. Overexpression ($\sim 30\%$) of several receptor tyrosine kinases in ErbB2 is associated with increasing breast cancer metastasis [2]. Magnetic resonance and ultrasound imaging, X-ray mammography, computed tomography, ELISA, and immunohistochemistry are the common methods to detect and quantify cancerous cells and tissues [3]. However, 80% of most breast cancers may not be detected by mammography due to the highly dense and proliferative cells. Moreover, large volume of samples and tagging molecules are required in ELISA and immunohistochemistry methods. Recently, numerous low-cost microfluidic sensors have been reported for cancer biomarker detection, demonstrating a great potential to realize rapid early-stage cancer diagnostics using only ultra-small sample consumptions without any complex and expensive procedures [4]. However, most of these sensors provide only a single modality of electrical, mechanical, electrochemical, or optical signal. With the continuing trend of minimizing sample consumptions, there will be an issue with the reliability and accuracy of biomarker detections associated with using low sample volumes available. Simultaneous generation of different sensing modalities from a single sensor may represent another method to improve reliability and reduce false (positive and negative) reads.

Label-free electrochemical sensors allow for rapid, and accurate detection and quantification of various chemical and biological species [5]. Micro/nanostructured materials have significant impacts on bio-recognition events and signal-transduction processes occurring at the electrochemical sensors, due to their large surface area, improved electron transport, and high electrochemical reactivity.⁴ The electrochemical electrodes, modified by these micro/nanomaterials, can provide the radial or spherical diffusion of the redox species from the bulk

solution to the surface of electrode, allowing for enhanced diffusion coefficient, as opposed to the slow, linear diffusion occurring at a planar or macro-electrode [6]. Therefore, the past two decades have witnessed a variety of high-performance electrochemical sensors modified by nanomaterials and nanostructures obtained using different synthesis methods, such as chemical vapor deposition, self-assembly, electrospinning hydrothermal, and phase separation [7]. However, owing to the generally inevitable non-uniformity in size, geometry and spatial distribution of the chemically synthesized nanostructures, performance reproducibility of a number of nanostructured electrochemical sensors (even using the same type of nanomaterial) needs to be improved.

Label-free plasmonic biosensors, made of noble-metal nanostructures, can detect minute amounts of biomolecules via detecting subtle changes in refractive index induced by specific molecular binding or absorption at the surfaces of sensors [8]. The index variations can be translated into resonant spectral shifts or power changes. For example, various gold (Au) nanostructures are used to conjugate with different biomolecules for the sensitive detection of cancer biomarkers [8]. However, similar to the electrochemical sensors, many plasmonic nanostructures (e.g., nanoplates, nanoparticles, and nanorods) are obtained by non-lithographical fabrication methods. To attain spatial and structural uniformity of the plasmonic nanostructures [9], sophisticated nanofabrication techniques were adopted, such as electron-beam lithography, focused ion beam machining, nanoimprinting, and hole mask colloidal lithography.

Here, we present a dual-modality sensor to detect and quantify cancer biomarkers with both electrochemical and plasmonic signals on a single microfluidic platform. The sensor can provide not only high reproducibility of detection performances, but also a desirable new ability to quantify specific biomarkers in a small sample volume using two different sensing mechanisms, thus perceiving benefits to improve detection reliability and reduce false positives and negatives. The sensor (Fig. 1) was formed by a periodic array of polymeric nanoposts coated with Au. Graphene oxide (GO) were assembled on the surfaces of the Au-coated nanoposts to facilitate biofunctionalization with antibody molecules. The electrochemical detection of the device provided several-fold enhancement of sensitivity for ErbB2 biomolecules, compared to a counterpart sensor using a planar electrode. The plasmonic detection of the sensor provided detailed information related to binding kinetics occurring at the sensor surface, which complemented the relatively low ability of the electrochemical sensor to study molecular interactions between antigen and antibody.

SENSOR PRINCIPLE AND STRUCTURE

In both the electrochemical and plasmonic modes of

operation, *ErbB2* solutions were injected to the sensor through the inlet of a microfluidic channel. The detection principle relies on the specific immuno-interactions between target *ErbB2* and anti-*ErbB2* on the surface of nanoposts. The electrochemical measurement includes monitoring the generated current flow from the Au nanoposts array to the counter Au electrode under an applied excitation potential between the Au nanoposts and Ag/AgCl electrodes. In the SPR measurement, coupling of incident light to the Au nanoposts provides a reflection dip owing to the excitation of (1, 0) surface plasmon polariton (SPP) at the air-Au nanoposts interface [10]. An increase in the concentration of *ErbB2* antigen molecules provides spectral shifts in SPR, as well as current changes in electrochemical measurement.

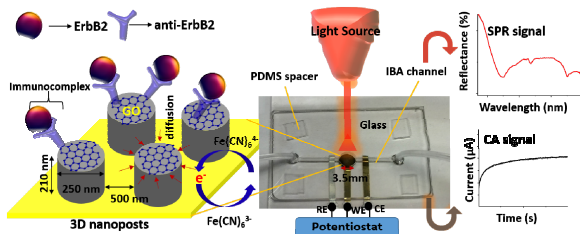


Figure 1: A pictorial image of a dual-modality microfluidic immunosensor for the detection of cancer biomarkers. -COOH groups are present at GO sheets that can facilitate *in-situ* immobilization of anti-*ErbB2* via forming amide bonds with -NH₂ groups of anti-*ErbB2*.

The sensor was fabricated using soft lithography based replica molding technique. At first, an array of nanoholes was formed in polydimethylsiloxane (PDMS) elastomer from a silicon stamp. Next, using a prepolymer solution (ZIPCONET™ UA or ZPUA), nanoposts were printed on a glass substrate from the PDMS mold. The obtained nanoposts have a period of 500 nm, a diameter of 250 nm, and a height of 210 nm. Further, an 80 nm thick layer of Au was deposited on the nanoposts by e-beam evaporation. Step-wise illustrations for the formation of the Au nanoposts is shown in Fig. 2(a-f). To form an electrochemical sensor, an Au counter electrode and a silver/silver chloride (Ag/AgCl) reference electrode were formed on the two sides of the Au nanoposts area. Finally, the three-electrode sensor was integrated with a microfluidic channel fabricated using an *in-situ* liquid phase polymerization (LP³) process [11]. In this process, 0.4 mm thick PDMS spacers were positioned between a 1 mm thick glass slide and the device substrate containing all electrodes to form an air cavity. A conventional milling machine with a 1-mm-diameter diamond drill bit was used to form the inlet and outlet holes through the top glass slide. Then, a photopatternable polymer consisting of isobornyl acrylate, tetraethylene glycol dimethacrylate, and 2, 2-dimethoxy-2-phenylacetophenone were mixed at a weight ratio of 31.66:1.66:1.0 [11]. This solution was injected to fill the air cavity. A photomask was positioned on top of the glass slide and UV light (12 mW/cm²) was used to expose the device for 60 s. The unpolymerized polymer was removed by rinsing the device in ethanol for

4 min, thus forming a microfluidic channel. Figure 2g-h show the SEM images show the fabricated Au nanoposts.

The surface functionalization of Au nanoposts was accomplished by self-assembling of GO nanosheets that facilitated covalent immobilization of anti-*ErbB2* due to the abundant functional groups (-CHO, -COOH etc.) at GO nanosheets. The GO assembled Au nanoposts was further functionalized with anti-*ErbB2* via EDC-NHS coupling chemistry. For immobilization, a mixer solution of anti-*ErbB2* (1 mg/mL) and EDC-NHS (EDC 0.2 M; NHS: 0.05 M) was prepared at 1:1 ratio. A 200 μ L solution of this mixer was injected to the surface of the GO-Au nanoposts through the inlet of the channel.

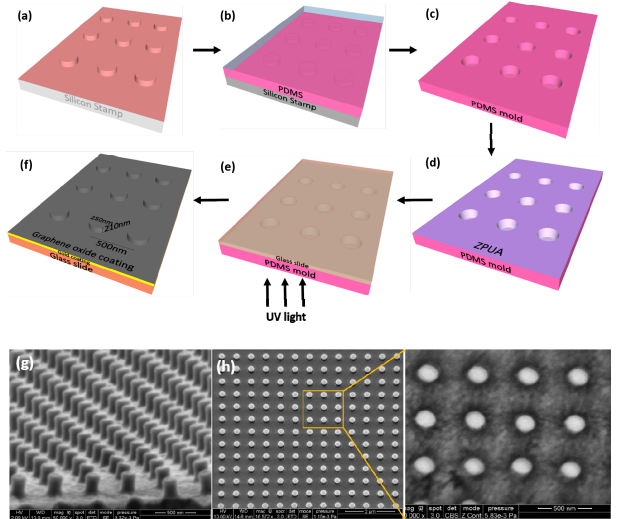


Figure 2: (a-f) Step-wise representation for the fabrication of 3D ZPUA nanoposts array using soft lithography-based replica molding process. (g-h) SEM images of the Au-coated nanoposts on a glass substrate.

RESULTS AND DISCUSSION

Chronoamperometric (CA) technique was employed to investigate the electrochemical redox reactivity that provided a transient current response of electrode with respect to time. Figure 3a shows the CA responses for the sensors made by Au nanoposts and planar Au (without nanoposts) wherein a five-fold enhancement of current is obtained with the Au nanoposts (~107 μ A) compared to that of the planar electrode (~19.7 μ A). This is because of the nanoposts that act as the nanoelectrodes enabling the radial or spherical diffusion of electrons [12]. However, the planar Au electrode enables linear diffusion resulting in a reduced redox current.

Next, this sensor was exploited to detect specific concentrations of biomarker (*ErbB2* antigen) using the CA technique. Several concentrations of *ErbB2* (1.0 fM to 0.1 μ M) were injected to nanoposts sensor. Figure 3 shows the CA responses as a function of *ErbB2* concentrations at a potential of 0.01 V for the sensors with and without incorporating the Au nanoposts. The sensor responses decrease with increasing *ErbB2* concentrations, due to the formation of immunocomplex between anti-*ErbB2* and *ErbB2* antigen that obstructs the acceleration of generated electrons from redox conversion. With increasing *ErbB2* concentration, the immunocomplex

layer becomes thicker leading to a reduction in the output current. Calibration plots exhibited that the sensor current is inversely proportional to the logarithmic concentration of *ErbB2* antigen (Fig. 3d). Approximately, a six-fold enhancement of sensitivity ($20.5 \mu\text{A}/\mu\text{M}/\text{cm}^2$) was obtained for the nanoposts-based sensor, compared to the control sensor without any nanoposts ($3.9 \mu\text{A}/\mu\text{M}/\text{cm}^2$). This is because of the larger surface area of the nanoposts and the radial diffusion of electrons towards the nanoposts. Abundant functional groups on the GO sheets also allowed an increased loading of antibody molecules, leading to the formation of more immunocomplex.

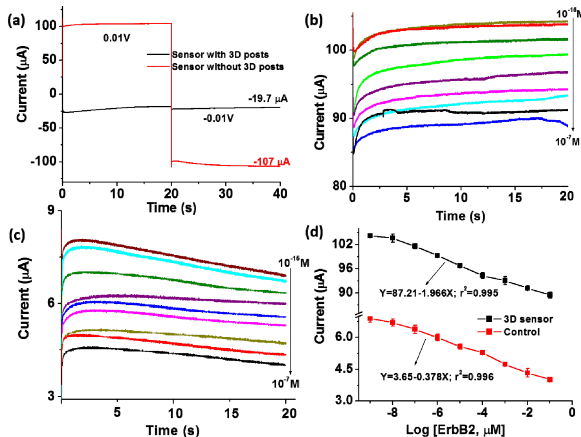


Figure 3: (a) Transient responses of the sensor with and without Au nanoposts. (b, c) CA responses for the sensors with (b) and without (c) nanoposts as a function of *ErbB2* concentration (10^{-15} to 10^{-7} M) at a constant sensing potential of 0.01 V in presence of PBS containing 5 mM of $[\text{Fe}(\text{CN})_6]^{3-/4-}$. (d) Calibration plots for the immunosensors.

The same sensor was also used for the SPR-based detection of *ErbB2* antigen. Coupling of incident light with the Au nanoposts introduced the SPR signal at the gold-air interface due to the vibration of free electrons at the Au surface [10]. The bulk refractive index sensitivity measurement of the sensor was performed by introducing water, acetone, ethanol, IPA, and chloroform on the sensor surface (Fig. 4a). The spectral shifts of the device in the presence of these chemicals is due to the changes in surrounding refractive index. The bulk index sensitivity of this sensor is found as 449.6 nm/RIU. The SPR spectra are shown for the Au nanoposts with and without GO coating, and after anti-*ErbB2* immobilization (Fig. 4b). After coating the device with a 49 nm thick layer of GO, a 17.7 nm red-shift in resonance wavelength was observed with respect to the bare structure having a resonance at 549 nm. This spectral shift is due to the incorporated GO layer which changes the refractive index at the sensor surface. When the sensor was exposed to the anti-*ErbB2* molecules, the wavelength of SPR resonance was further shifted to 704 nm, because of the increased dielectric constant of the environment resulting from the accumulation of polarization charges on the dielectric. Fig. 4c shows the SPR spectra for this sensor as a function of *ErbB2* concentrations (1×10^{-15} M to 1×10^{-9} M) in PBS solution (pH = 7.4). When the anti-*ErbB2* conjugated

nanoposts array was excited by the incident light, a reflection dip was found at a resonance wavelength of 716.5 nm for 1.0 fM concentration of *ErbB2*. This is due to the antigen-antibody interaction on the plasmonic surface that enhances the refractive index at the sensor surface. As the *ErbB2* concentration increased from 1 fM to 1 nM, the resonance wavelengths were redshifted from 716.5 to 719.5 nm. Figure 4d shows the sensor calibration plot between the logarithm concentrations of *ErbB2* and the resonance wavelengths. This SPR sensor shows a sensitivity of 2.9 nm/RIU within the low concentration range of *ErbB2* biomarker (1×10^{-15} M to 1×10^{-9} M). A transient response to track dynamically the minute amount of *ErbB2* molecules at concentrations of 1×10^{-14} M and 1×10^{-13} M is shown in Fig. 4c. When the sensor was exposed to the PBS solution (baseline), it provided a stable resonance wavelength of 699.3 nm after which the sensor was exposed with *ErbB2* (1×10^{-14} M) molecules. This is termed as association phase that provided a redshift of 4.9 nm. By varying the *ErbB2* concentration from 1×10^{-14} M to 1×10^{-13} M, this sensor further provided a redshift of 0.18 nm (association phase). In the dissociation phase, the sensor was treated with the PBS solution and the signal decreased due to washing off the weekly bound *ErbB2* molecules from the sensor surface.

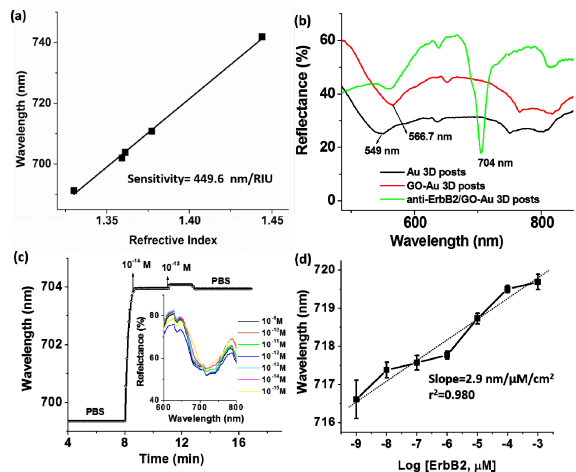


Figure 4: (a) Refractive index sensitivity of the sensor. (b) SPR response showing a redshift of 17.7 nm after coating GO on Au nanoposts. With anti-*ErbB2* on GO-Au nanoposts, the resonance is redshifted to 716.6 nm, (c) Transient response for detection of *ErbB2*. The inset shows the full spectra dependence of *ErbB2* concentration (10^{-15} to 10^{-9} M). (d) SPR resonance wavelengths as a function of *ErbB2* concentration.

To estimate the selectivity, this sensor was tested with similar species such as *ErbB3* and *ErbB4* (Fig. 5a-b). When *ErbB2* antigen (1.0 fM) was added to the nonspecific *ErbB3*, *ErbB4*, and a mixture of *ErbB3* and *ErbB4*, the sensor response did not change significantly, as evident by its low relative standard deviation (RSD; $\pm 0.11\%$). The sensor also shows a low RSD of $\pm 1.07\%$ without the *ErbB2* antigen. Moreover, the reproducibility tests were conducted using four identical sensors. The measurement revealed high reproducibility with a minute deviation from initial signal (RSD: $\pm 1.95\%$, Fig. 5c). The high reproducibility of this sensor is due to the periodic

and uniform assembly of the Au nanoposts. Lastly, the sensor exhibited a stable amperometric signature for a four-week measurement (Fig. 5d).

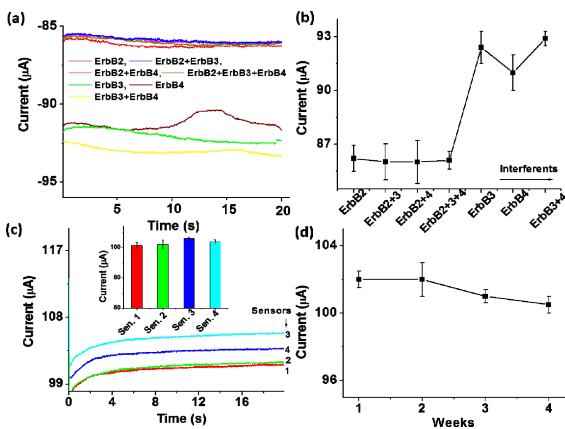


Figure 5: (a) Transient responses for selectivity test of the sensor in presence of nonspecific (ErbB receptor tyrosine kinase family) interferents such as ErbB3 (1.0 nM) and ErbB4 (1.0 nM). Concentration of ErbB2 was set to 1fM during this selectivity test. (b) Current versus interferents. (c) Reproducibility test of the sensor conducted with four identical immunoelectrodes with 1.0 fM concentration of ErbB2. (d) Stability test of this sensor performed for 4 weeks at an interval of seven days.

Table 1 compares the performances of this dual-modality sensor with other reported immunosensors. The electrochemical measurement of the sensor offered a higher sensitivity ($20.5 \mu\text{A } \mu\text{M}^{-1}$) than those using other nanostructured materials such as graphene foam-TiO₂ nanofibers ($0.585 \mu\text{A } \mu\text{M}^{-1}$)[3] and ZnO nanowires ($6.36 \text{nA } \mu\text{M}^{-1}$)[14]. The plasmonic measurement of the sensor provides a competitive detection range, compared to other reported sensors. In addition, the SPR mode allows tracking the associations and dissociations of biomarker molecules, which complements the weak ability of electrochemical detection mode in this regard.

Table 1. Comparisons of device performances.

Electrodes	Biomarkers	Sensitivity	Test range
GF-nTiO ₂ ^[3]	ErbB2	$0.585 \mu\text{A } \mu\text{M}^{-1}$	1.0 fM–0.1 μM
Ring resonator ^[13]	HER2	30 nm/RIU	$189.5 \text{ pM}-1.46 \text{ nM}$
ZnO nanowires ^[14]	BRCA1	$6.36 \text{nA } \mu\text{M}^{-1}$	$10.0-100.0 \mu\text{M}$
Graphene sheets ^[15]	Carcinoembryonic antigen	$0.1 \mu\text{A } \mu\text{M}^{-1}$	$2.7-333.3 \text{ pM}$
Au nanoposts (this work)	ErbB2	$20.5 \mu\text{A } \mu\text{M}^{-1}$ $2.9 \text{ nm}/\mu\text{M}/\text{cm}^2$	1.0 fM–1 nM 1.0 fM–1 nM

CONCLUSIONS

A low-cost, highly efficient, and dual-modality sensor has been demonstrated for the detection of cancer biomarkers using both the electrochemical and SPR sensing mechanisms. The larger surface area of the Au nanoposts allows for the sufficient attachment of antibodies to the sensor surface. In the electrochemical mode, the nanoposts enables the radial diffusion of electrons resulting in a several-fold higher sensitivity compared to the bulk electrode without nanoposts. In the

SPR mode, the sensor allows easy tracking of the associations and dissociations of biomarker molecules at the sensor surface. Compared to the sensors using synthesized nanomaterials, this sensor offers higher reproducibility due to using the ordered and uniform nanostructures. Therefore, the dual-modality performance of the sensor provides a new approach to improve detection reliability and false alarm immunity for breast cancer detection.

ACKNOWLEDGEMENTS

This work was supported in part by the National Science Foundation under grants # DBI-1353819, CCF-1331390, 461 IIP-1602089, and IOS-1650182.

REFERENCES

- [1] J. Wang, "Electrochemical Biosensors: Towards Point-of-Care Cancer Diagnostics", *Biosens. Bioelectron.*, vol. 21, pp. 1887–1892, 2006.
- [2] I. E. Tothill, "Biosensors for Cancer Markers Diagnosis", *Semin. Cell Dev. Biol.* 2009, 20, 55–62.
- [3] Md. A. Ali, K. Mondal , Y. Jiao, S. Oren, Z. Xu, A. Sharma, L. Dong, "Microfluidic Immuno-Biochip for Detection of Breast Cancer Biomarkers Using Hierarchical Composite of Porous Graphene and Titanium Dioxide Nanofibers", *ACS Appl. Mater. Interfaces*, vol. 8, pp. 20570–20582, 2016.
- [4] H. Li, J. He, S. Li, A. P. Turner, "Electrochemical Immunosensor with N-doped Graphene-Modified Electrode for Label-Free Detection of the Breast Cancer Biomarker CA 15-3", *Biosens. Bioelectron.* vol. 43, pp. 25–29, 2013.
- [5] Z. Gao, H. Deng, W. Shen, Y. Ren "A Label-Free Biosensor for Electrochemical Detection of Femtomolar microRNAs" *Anal. Chem.*, vol. 85, pp. 1624–1630, 2013.
- [6] J. Heinze, "Ultramicroelectrodes in Electrochemistry", *Angew. Chem. Int. Ed. Engl.*, vol. 32, pp. 1268–1288, 1993.
- [7] M. Holzinger, A. Le Goff, S. Cosnier "Nanomaterials for Biosensing Applications: A Review", *Front. Chem.*, vol. 2, pp. 63, 2014.
- [8] G. J. Nusz, A. C. Curry, S. M. Marinakos, A. Wax, A. Chilkoti, "Rational Selection of Gold Nanorod Geometry for Label-Free Plasmonic Biosensors", *ACS Nano*, vol. 3, pp. 795–806, 2009.
- [9] M. E. Stewart, C. R. Anderton, L. B. Thompson, J. Maria, S. K. Gray, J. A. Rogers, R. G. Nuzzo, "Nanostructured Plasmonic Sensors", *Chem. Rev.*, vol. 108, pp. 494–521, 2008.
- [10] Q. Wang, W. Han, P. Liu, and L. Dong, "Electrically Tunable Quasi-3D Mushroom Plasmonic Crystal", *J. Lightw. Technol.*, vol. 34, pp. 2175–2181, 2015.
- [11] D. J. Beebe, J. S. Moore, Q. Yu, R. H. Liu, M. L. Kraft, B.-H. Jo, C. Devadoss, "Microfluidic tectonics: A comprehensive construction platform for microfluidic systems", *Proc. Natl. Acad. Sci.*, vol. 97, pp. 13488–93, 2000.
- [12] M. E. Sandison, J. M. Cooper, "Nanofabrication of Electrode Arrays by Electron-Beam and Nanoimprint Lithographies", *Lab Chip*, vol. 6, pp. 1020–5, 2006.
- [13] J. T. Gohring, P. S. Dale, X. Fan, "Detection of HER2 Breast Cancer Biomarker Using the Opto-Fluidic Ring Resonator Biosensor", *Sens. Actuat. B*, vol. 146, pp. 226–30, 2010.
- [14] N. A. Mansor, Z. M. Zain, H. H. Hamzah, *et al.*, "Detection of Breast Cancer 1 (BRCA1) Gene Using an Electrochemical DNA Biosensor Based on Immobilized ZnO Nanowires", *Open J. Appl. Biosens.* vol. 3, pp. 9–17, 2014.
- [15] X. Chen, X. Jia, J. Han, J. Ma, Z. Ma "Electrochemical Immunosensor for Simultaneous Detection of Multiplex Cancer Biomarkers Based on Graphene Nanocomposites", *Biosens. Bioelectron.*, vol. 50, pp. 356–361, 2013.

CONTACT

*L. Dong, tel: +1- 515-294-0388; ldong@iastate.edu